Modeling of wall condensation in the presence of noncondensable light gas

S. Benteboula, F. Dabbene

Version of Record: https://www.sciencedirect.com/science/article/pii/S0017931019350537
Manuscript_6b0500141e10a612d11d78250c7855e2

Modeling of wall condensation in the presence of noncondensable light gas

S. Benteboula[1], F. Dabbene

CEA Paris-Saclay, 91191, Gif-Sur-Yvette Cedex

Abstract

During a loss of coolant accident in nuclear reactor, significant amounts of steam and hydrogen can be released in the containment. Condensation of steam in the presence of noncondensable gases on the containment walls and structures is a key issue because of its role in removing heat from the atmosphere. Extensive experimental and theoretical studies have been carried out for a better understanding of this complex phenomenon which involves several physical processes and parameters. When condensation takes place in the presence of noncondensable gases a liquid film is formed and noncondensable gases accumulate at the interface. The diffusion of steam through the gaseous layer depends on the gas composition, velocity, temperature and pressure. The formation of a gaseous layer leads to a significant reduction of heat transfer. Simulations based on CFD or lumped parameter (LP) approaches use correlations to estimate heat and mass transfer due to condensation. In this work, we are interested in theoretical correlations based on the diffusion layer theory using heat and mass transfer analogy. Among the variables and parameters affecting wall condensation, the effect of the gas mixture properties in particular the diffusion coefficient modeling is investigated. Test cases of steam injection into an enclosure filled with air or air-hydrogen mixture are simulated with a LP code using two different correlations for the evaluation of heat and mass transfer. Each correlation is based on different formulations of the effective diffusion coefficient. The ISP47 test performed in the MISTRA facility was used for validation purpose. The results showed that the addressed heat and mass transfer correlations underestimate the

[☆]Fully documented templates are available in the elsarticle package on CTAN.

[1]sonia.benteboula@cea.fr

condensation rate in the steady state. Furthermore, the impact of the effective diffusion coefficient modeling on the heat and mass transfer turned out to be significant compared to the effect of the heat and mass transfer correlation.

Keywords: Film condensation, heat and mass transfer analogy, diffusion boundary layer, noncondensable light gas, effective diffusion coefficient.

---

1. Introduction

In the course of a postulated accident in a light water nuclear reactor LWR, large amounts of steam are released in the containment. The mass and energy supply from the break leading to the pressurization and heat up of the atmosphere, could threaten the containment integrity. Hydrogen can be released, in the case of severe accident, in the containment due to the core meltdown and its accumulation could likely result in deflagration or detonation under certain conditions. Heat is transferred to the containment atmosphere, internal structures and external walls mainly by condensation and, to a lesser extent, by convection which affects the pressure evolution and the hydrogen distribution within the containment. By removing heat, condensation plays an important role in mitigating the containment pressure. However, it also affects the mixing process and could lead to local hydrogen accumulation, which is a dangerous issue for containment safety.

Condensation in the presence of noncondensable gases is a complex process involving several physical phenomena and parameters such as: circulation pattern, flow regime, composition of the atmosphere and mixing process, thermodynamic variables, geometry, wall characteristics and orientation. Numerous theoretical and experimental studies have been conducted on condensation in the last decades for further understanding of this phenomenon and better prediction of the associated heat and mass transfer rates.

From theoretical point of view, one can mention the pioneer work of Nusselt [1] on the modeling of film condensation of saturated steam on vertical plate. Improvements of this model have been introduced in the following works [2], [3], [4] and [5] to take into account, for instance, the effective latent heat including sensible heat transfer, the inertial forces and convection energy in condensate film.

In the presence of noncondensable gases, Sparrow and Lin [6] proposed a model based on the mass, momentum and energy conservation equations for

the liquid film and the diffusion gaseous layer which is formed on the liquid film interface. The effects of superheating, interfacial resistance, thermo-diffusion and diffusion-thermo have been taken into account in this model in the work of [7]. Rose [8] proposed similarity solution of the system of equations given in [7] assuming constant the physical properties and by imposing the velocity and concentration profiles in the boundary layer. These studies showed that condensation rate and heat transfer can significantly be reduced by a small amount of noncondensable gases.

Solving the conservation equations in the gas boundary layer and in the liquid layer at the reactor scale may be very costly, from computing performances point of view, when dealing with accident scenarios in the containment. In thermal-hydraulics codes using lumped parameter or CFD methods, the approaches are often limited to the determination of the condensation heat and mass transfer coefficients and the involved parameters with correlations. Due to their significantly reduced computational time, the LP codes are commonly used in safety analysis. This approach might be more suitable compared to CFD for the prediction of the global variables such as pressure. Nevertheless, it presents some limitations regarding the local distribution of the flow variables since the inertial and diffusion terms are not considered. The models for heat and mass transfer coefficients adopted in LP codes are developed basing on experimental observations or on the heat and mass transfer analogy (HMTA) method. A table highlighting a selection of these models is presented in Appendix A.

Among correlations based on experiments, Uchida [9] and Tagami [10] correlations are usually used in safety codes owing to their simplicity and conservatism. In the Uchida correlation proposed for natural convection in steady state, the heat transfer coefficient (HTC) is a function of the interface to the bulk densities ratio. When in Tagami correlation used for the containment design, a time-dependent expression of HTC is proposed during the first phase of blow-down and the Uchida's HTC is used in the next phase. Later on, many authors proposed correlations taking into account other physical parameters such as the pressure and the wall-to-bulk temperature difference in Dehbi correlation [11].

Theoretical models based on heat and mass transfer analogy can be referred into two categories. Models developed using molar fluxes, where the driving force is expressed in terms of partial pressures or molar fractions, such as in the original model of Chilton-Colburn [12] and several authors like Bird [13] and Collier [14]. The second formulation is based on the mass

fluxes such as proposed in [15] or [16].

In the Collier-Stephan correlation [14], authors considered a low mass transfer rate and assumed that the convective term for noncondensable gas towards the interface is of the same order of magnitude as the diffusion term towards the bulk flow. A simple model has been proposed by [17] for forced convection condensation for a turbulent boundary layer of an air-steam mixture by considering a smooth liquid-steam interface. This model has been modified in [18] to be applied to natural convection regime and the resistance of the liquid film was neglected. This model was validated using the Uchida and Tagami experimental results. It has been shown, that the film resistance becomes negligible compared to that of the noncondensable gas layer when the air mass fraction exceeds 10%. Both forced and natural convection modes were taken into account in the heat, momentum and mass transfer (HMMT) model developed in [19]. The effect of the wavy liquid-film structure was taken into account, that improves steam transport in the diffusion layer of the air-steam mixture. The validation was performed on tests representative of containment accident case conducted in the CVTR facility. The model developed by [20] is derived from the Collier-Stephan approach where the Clausius-Clapeyron equation was solved to obtain a condensation conductivity with approximations for the steam properties and perfect gas law for noncondensable gases. The case of steam condensation in a tube was studied using this model in [21]. The thermal resistance of the liquid film and its wave structure were taken into account in the model developed by [22]. In this model based on the diffusion layer theory using the HMT analogy, the effect of wall inclination is introduced in the determination of the liquid film HTC. The suction effect is taken into account in the Sherwood number definition.

Several adaptations of models using the analogy method have been developed according to the applications. In the COPAIN correlation [23], a correction factor is introduced in both convective and condensation HTC formulations to account, among others, for the suction effect for better fitting with measurements of the COPAIN experimental program. A new correction factor has been proposed for the total HTC with adaptation of this coefficient to cover a large number of experiments of the literature for air-steam mixture in in [24] and in presence of light gas in [25]. It should be recalled that the analogy between mass transfer and energy transfer is also used in CFD approach computations, for example [26]. In this last work, the inclination of the wall is taken into account in the film resistance.

Separate and integral effect tests have been carried out for better understanding of the involved physical phenomena and for the validation of the containment CFD or LP computational codes. To this aim, a set of tests were performed in the MISTRA facility in the framework of ISP47 exercise [27]. The selected test, includes phases which are representative of the containment atmosphere evolution in the case of severe accident. The first phase is the containment pressurization by the injection of superheated steam. The second phase consists in injecting helium to simulate hydrogen release in the core degradation phase.

In the present work we investigate the influence of the effective diffusion coefficient modeling on the global heat and mass transfer through two different condensation correlations. First, we give a brief description of the lumped-parameter CAST3M-LP code developed in CEA. Then we recall some correlations based on the diffusion theory layer and heat and mass transfer analogy. Models for determination of the binary and the effective diffusion coefficients are given. After that, the test cases used for the models assessment and the ISP47 test for validation are described and results are discussed.

2. Heat and mass transfer modeling

In this study, we are interested in correlations for condensation in the presence of noncondensable gases based on the heat and mass transfer analogy. These two correlations called Chilton and COPAIN are used in the framework of lumped parameter approach and are implemented in the CAST3M-LP containment code.

Let's recall, that variables and parameters used in the heat and mass transfer correlations, for example the interface and bulk temperatures and the gas mixture properties, are often determined in different ways. In addition, the validity of the analogy of heat and mass transfer is restricted to dilute concentrations of steam (the diffusive component) [28]. When high mass fluxes are involved, the introduction of a corrective factor to account for suction effect could improve the predictivity of the analogy based models as mentioned in [13] and [29].

2.1. CAST3M-LP code description

The CAST3M-LP code is based on a lumped-parameter approach which consists in representing the containment free volume with a group of sub-volumes, called compartments or zones. These compartments could be in

Nomenclature

C_p	specific heat at constant pressure [J/kg/K]
D	diffusion coefficient [m^2/s]
g	gravity acceleration [m/s^2]
h	heat transfer coefficient [$W/m^2/K$]
h_{fg}	latent heat of vaporization [J/kg]
k_{cd}	mass transfer coefficient [m/s]
L	characteristic length [m]
$\dot{m}''$	mass flux [$kg/m^2/s$]
m	mass [kg]
P	pressure [Pa]
q	heat flux [W/m^2]
R_v	specific gas constant for steam [J/kg/K]
T	temperature [K]
t	time [s]
v	velocity [m/s]
X	mole fraction [-]
Y	mass fraction [-]
W	molecular weight [kg]

Greek letters

α	thermal diffusivity [m^2/s]
δ	liquid film thickness [m]
δ_d	diffusion layer thickness [m]
ΔT	temperature difference [K]
λ	thermal conductivity [W/m/K]
μ	dynamic viscosity [kg/m/s]
ν	kinematic viscosity [m^2/s]
ρ	density [kg/m^3]
τ	stress tensor [Pa]
Θ	correction factor [-]

Subscripts/Superscripts

b	bulk flow
cd	condensation
cv	convection
ext	surrounding media
f	film condensate
g	gas mixture
h	hybrid
i	interface
j	species
nc	noncondensable gas
sat	saturated state
v	vapor
w	wall

Dimensionless numbers

Gr	Grashof number
Nu	Nusselt number
Pr	Prandtl number
Re	Reynolds number
Sc	Schmidt number
Sh	Sherwood number

Abbreviations

HMT	heat and mass transfer
HTC	heat transfer coefficient
LP	lumped parameter

contact or not of solid walls. A sump is associated to each volume to collect water of liquid sources from injection, bulk condensation and wall condensation. The compartments are connected to each others through atmospheric junctions and the sumps are connected through liquid junctions. The mathematical model assumes that the flow field variables are uniformly distributed in space for each sub-volume and correspond to their average values. Thermodynamic quantities are then obtained by solving for each sub-volume the integral mass and energy conservation equations. The mass flowrate in the atmospheric junctions is determined from a simplified momentum balance equation. Heat and mass transfer on walls are determined by correlation based on experiments (Uchida [9] and Tagami [10]) or using heat and mass transfer analogy method (Chilton in [30], [31] and COPAIN [23]). These correlations rely on the wall temperature which is obtained by solving the one dimensional conduction equation in the wall thickness. Among the validation test basis of the CAST3M-LP code, experimental tests performed in MISTRA facility involving steam condensation in presence of air and light gas (helium) have been calculated using Chilton correlation in order to set-up an optimized nodalization scheme [32].

2.2. Heat and mass transfer correlations

Chilton and COPAIN correlations are established in the turbulent convection regime and are used here considering natural circulation pattern. The following hypotheses have been made.

1. A saturated state is assumed at the steam-liquid interface ($P_{v,i} = P_{sat}(T_i)$).
2. The thermal resistance of the liquid film is neglected, so as the interface temperature is equal to the wall temperature ($T_i = T_w$).
3. The perfect gas law is used to estimate the density of noncondensable gases at the interface ($\rho_{nc,i} = (P_{tot} - P_{v,i})/(r_{nc,i}\, T_i)$).
4. The physical properties of the gas mixture are determined at the bulk temperature.
5. The composition of noncondensable gas mixture at the interface is identical to that in the bulk.

It's worth noting that these correlations involve further models to determine the gas mixture physical properties such as the diffusion coefficient, viscosity and conductivity.

The heat flux on walls, q_w, is composed of a sensible heat flux of convection q_{cv} and a latent heat flux of condensation q_{cd}:

$$\begin{aligned} q_w &= q_{cv} + q_{cd} = h_{tot}\,(T_b - T_w), && (1)\\ q_{cv} &= h_{cv}\,(T_b - T_w), && (2)\\ q_{cd} &= \dot{m}''_{v,i}\,(h_{v,b} - h_{l,w}) = h_{cd}\,(T_b - T_w). && (3) \end{aligned}$$

where $h_{v,b} = h_v(P_{v,b}, T_b)$ is the steam enthalpy at the bulk conditions and $h_{l,w} = h_l(P_{tot}, T_w)$ the liquid enthalpy at the total pressure and the wall temperature. In equation (1), the radiation heat transfer is not taken into account even if it could have significant effect under certain conditions [33].

The condensation mass flux $\dot{m}''_{v,i}$ through the diffusion layer defined by

$$\dot{m}''_{v,i} = -\frac{\rho\, D}{1 - Y_{v,i}} \left(\frac{\partial Y_{v,i}}{\partial y} \right) \tag{4}$$

can be written as a function of the mass transfer coefficient k_{cd}

$$\dot{m}''_{v,i} = k_{cd} \frac{\rho\,(Y_{v,b} - Y_{v,i})}{1 - Y_{v,i}}. \tag{5}$$

2.2.1. Chilton correlation

The Chilton correlation implemented in the CAST3M-LP code is based on the Chilton-Colburn analogy [14] which gives the mass transfer coefficient depending on the heat transfer one.

$$k_{cd} = h_{cv} (\rho\, C_p)^{-1/3} \left(\frac{\mathrm{Pr}}{\mathrm{Sc}} \right)^{2/3}. \tag{6}$$

The convection heat transfer coefficient h_{cv} is written as a function of the Nusselt number and analogously the specific mass transfer coefficient k_{cd} as a function of the Sherwood number

$$h_{cv} = \frac{\lambda\, \mathrm{Nu}}{L}, \tag{7}$$

$$k_{cd} = \frac{D\, \mathrm{Sh}}{L}. \tag{8}$$

The Nusselt number is determined with the Mac-Adams correlation for free convection on vertical plate and the Sherwood number by applying the HMT analogy

$$\mathrm{Nu} = 0.13\,(\mathrm{Gr}\,\mathrm{Pr})^{1/3}, \tag{9}$$
$$\mathrm{Sh} = 0.13\,(\mathrm{Gr}\,\mathrm{Sc})^{1/3}. \tag{10}$$

The Prandtl, Schmidt and Grashof numbers are based on the gas properties in the bulk.

$$\mathrm{Pr} = \frac{\mu}{\rho\,\alpha},\ \ \mathrm{Sc} = \frac{\mu}{\rho\,D},\ \ \mathrm{Gr} = \rho\,g\frac{\rho_w - \rho}{\mu^2}L^3. \tag{11}$$

Note that the Grashof number is written in terms of density.
Finally, assuming a Prandtl number of 1, the h_{cv} and k_{cd} coefficients can be written

$$h_{cv} = 0.13\,\lambda\left(g\,\rho\,\frac{\rho_w - \rho}{\mu^2}\right)^{1/3}, \tag{12}$$
$$k_{cd} = \frac{D^{2/3}}{\lambda}\left(\frac{\mu}{\rho}\right)^{1/3} h_{cv}. \tag{13}$$

2.2.2. COPAIN correlation

The COPAIN correlation has been developed in the framework of the experimental program carried out in the CEA on wall condensation in the COPAIN facility [34]. The detailed and accurate data have been provided in [23] for condensation in the presence of noncondensable gases for a wide range of parameters which are summarized in table 1. The condensing plate of 2 m long and 0.6 m wide is placed vertically in a rectangular channel of $0.6 \times 0.5\,\mathrm{m}^2$ cross section.

P [bar]	1.0 - 1.2 - 4.0 - 6.7
Y_{nc} [−]	0.1 - 0.3 - 0.4 - 0.5 - 0.88 - 1.0
U_{inlet} [m/s]	0.1 - 0.3 - 0.5 - 1.0 - 2.0 - 3.0
X_{He}/X_{nc} [-]	0.0 - 0.1 - 0.4 - 1.0
$(T_v - T_{sat})$ $[K]$	10 - 20 - 40
ϕ [kW/m^2]	1 - 5 - 10 - 25

Table 1: Operating conditions of COPAIN tests.

This correlation is also based on HMT analogy and the heat and mass transfer coefficients are written as a function of the Nusselt (Nu) and Sherwood (Sh) numbers respectively. The main differences with the Chilton correlation are, first, the introduction of a correction factor θ proposed in [23] in order to overcome the lack of modeling such as the suction and the film effects, and second, the Prandtl number is not imposed equal to one.

Thus, the modified Nusselt and Sherwood numbers based on Mac-Adams correlation are given by

$$\mathrm{Nu} = 0.13\,\theta\,(\mathrm{Gr_h}\,\mathrm{Pr})^{1/3},\ \ \mathrm{Sh} = 0.13\,\theta\,(\mathrm{Gr_h}\,\mathrm{Sc})^{1/3},$$

where $\mathrm{Gr_h}$ is the hybrid Grashof number defined by

$$\mathrm{Gr_h} = \frac{\rho^2\,g L^3}{\mu^2}\left(1 - \frac{T_w}{T_b} + \frac{Y_{nc,i} - Y_{nc,b}}{\frac{W_{nc}}{W_{nc}-W_v} - Y_{nc,b}}\right). \tag{14}$$

The Pr and Sc numbers are given in equation (11), and the correction factor introduced to fit the experimental data for a wide range of parameters given in table 1 is determined by

$$\theta = 0.8254 + 0.616\frac{X_{nc,i} - X_{nc,b}}{X_{nc,i}}. \tag{15}$$

2.3. The effective diffusion coefficient

Several models have been used in literature to estimate the effective diffusion coefficient of steam in the gas mixture noted $D_{v,\,nc}$ or $D_{v,\,g}$. Furthermore, different formulations are used to determine the binary diffusion coefficient noted D_v^j.

Among these models, the most commonly used in the literature is the Wilke's method [35] given by the following equation

$$D_{v,\,nc} = \frac{1 - X_v}{\sum_{j,j\neq v}\left(X^j/D_v^j\right)}. \tag{16}$$

Some authors [36] use mass fractions for the diffusion coefficient evaluation

$$D_{v,\,nc} = \frac{1 - Y_v}{\sum_{j,j\neq v}\left(Y^j/D_v^j\right)}. \tag{17}$$

In [37], the diffusion coefficient is given by the so-called Blanc law

$$D_{v,\,nc} = \frac{1 - Y_v}{\sum_{j, j \neq v} \left(X^j / D_v^j \right)}, \tag{18}$$

In the containment code RALOC [30], the diffusion coefficient is determined by

$$D_{v,\,g} = \frac{1}{\sum_j \left(X^j / D_v^j \right)}. \tag{19}$$

Here g refers to the gas mixture including the steam and nc to the noncondensable gas mixture. It should be noted that, in this work, the mass and mole fractions are determined at the bulk conditions. In the literature [22, 36], the gas properties can be evaluated at the diffusion layer with several definitions of the average temperature.

2.3.1. Model-1

From kinetic theory of gases, at low and moderate pressures, binary diffusion coefficients in gas vary inversely with pressure or density and they are independent of the mixture composition.

The binary diffusion coefficient is estimated with the following equation

$$D_v^j(P, T) = \frac{a}{10^{-5}\, P} \left(\frac{T}{273.15} \right)^n, \tag{20}$$

where the coefficients a and n associated to each species are reported in table 2.

The effective diffusion coefficient $D_{v,g}$ is determined by equation (19) including the steam self-diffusion.

This model is used in the Chilton correlation of the containment code RALOC [30].

2.3.2. Model-2

In this model, the binary diffusion coefficient of the vapor v in a species j, is determined by the Fuller correlation [38] :

$$D_v^j(P, T) = \frac{0.0143\, T^{1.75}}{P (10^3\, W_{v,j})^{1/2} \left[(\Sigma_v)_v^{1/3} + (\Sigma_v)_j^{1/3} \right]^2}, \tag{21}$$

By definition

$$W_{v,j} = 2\, (1/W_v + 1/W_j)^{-1}. \tag{22}$$

gas	H2O	N2	O2	He	H2
a	$2.77.10^{-5}$	$2.27.10^{-5}$	$2.40.10^{-5}$	$7.30.10^{-5}$	$7.80.10^{-5}$
n	0.0	1.75	1.71	1.75	1.75
Σ_v	13.1	18.5	16.3	2.67	6.12

Table 2: Coefficients for binary diffusivities estimation. Σ_v is the volumetric diffusion for different species.

The effective diffusion coefficient $D_{v,nc}$ is determined by equation (16).

Similarly to the above formulation of the binary diffusion coefficient in equation (20), the fuller model (21) can be re-written as

$$D_v^j = \frac{a'}{10^{-5}\,P}\left(\frac{T}{273.15}\right)^{1.75}, \tag{23}$$

with the coefficient a' given in table 3.

gas	H2O	N2	O2	He	H2
a'	$2.78.10^{-5}$	$2.24.10^{-5}$	$2.28.10^{-5}$	$7.31.10^{-5}$	$7.86.10^{-5}$

Table 3: Coefficients for binary diffusivities estimation. Σ_v is the volumetric diffusion for different species.

Note that, the main differences concern the steam self-diffusion, which is depending here on both pressure and temperature, and the power coefficient for the oxygen species.

2.3.3. Model-3

The third model combines the Fuller correlation (21) for the binary diffusion coefficient and the effective diffusion coefficient based on the mass fractions given by equation (17). This formulation is used in the COPAIN heat and mass transfer correlation of the CEA code called CATHARE.

3. Analytic tests

We are interested in the behavior of the condensation heat and mass transfer in the presence of noncondensable gases in particular the effect of light gas. The presence of light gas such as hydrogen in the atmosphere composition can be representative of severe accident situation. For that, two simplified test-cases consisting of steam injection into an enclosure, initially

filled with air for Test-1 and with air-hydrogen mixture for Test-2, are addressed. The aim is to highlight the influence of the effective diffusion coefficient modeling on the global heat and mass transfer in both transient and steady regimes, and that, in presence or not of light gas.

3.1. Binary air-steam mixture

3.1.1. Test-1: steam injection in air

Homogeneous initial conditions are considered in a cylindrical enclosure of $20\,\mathrm{m}^3$ of volume filled with 28.41 kg of air at the following thermodynamic conditions: $P_0 = 1.2\,\mathrm{bar}$ and $T_0 = 45℃$. The condensation surface of $42.026\,\mathrm{m}^2$ is the enclosure wall maintained at constant temperature $T_w = 45℃$. A superheated steam is injected in the enclosure with a constant mass flowrate of $200\,\mathrm{g/s}$ and constant temperature of 200℃ during 1000 s. The calculations are carried out for a duration of 2000 s. These durations are chosen in order to observe the steady states during and after the steam injection. The first steady state is reached when the injected mass and energy are balanced by the heat and mass transfer to the wall and by bulk condensation. After the end of injection, the gas temperature decreases to attain the wall temperature with a final pressure corresponding to the saturation conditions.

3.1.2. Test-1 results

Calculations have been performed with two different correlations for heat and mass transfer coefficient (Chilton and COPAIN), described in paragraph 2.2. Each HMT correlation used three different models for the determination of the effective diffusion coefficient given in paragraph 2.3 and referred by 1, 2 and 3 in the figure's captions.

The effective diffusion coefficient. Let us notice that the mixture law for D_v in model-1 Eq.19 takes into account the presence of steam in the gaseous diffusion layer while model-2 and model-3 assume that steam diffuses through a layer of noncondensable gases. In Fig. 1, the effective diffusion coefficient D_v is compared for each case. This quantity depends on pressure, temperature and gas composition. During the steam injection phase corresponding to $t \leq 1000\,\mathrm{s}$, a lower D_v is obtained with model-1 due to the contribution of the steam self-diffusion which is inversely proportional to the pressure. A rise of D_v is observed at the end of the steam injection due to the significant reduction of steam content. Model-2 and model-3 give the same evolution since the effective diffusion coefficient D_v for a binary air-steam mixture is

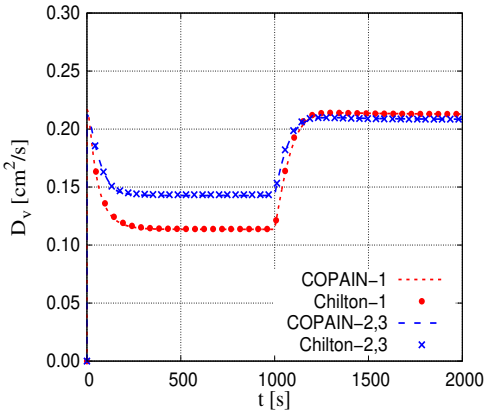

Figure 1: Test-1. Time evolution of the effective diffusion D_v using COPAIN and Chilton correlation with three different models for D_v.

reduced to the binary diffusion coefficient D_v^{air} given by equation (21). In these last cases, the D_v evolution is proportional to the ratio $T^{1.75}/P$ which decreases and reaches a constant value at the steady state as the steam is injected and inversely in the post-injection phase. No influence of the heat and mass transfer correlation is observed, so similar results are obtained with COPAIN and Chilton correlations for the same model of D_v.

Heat flux. The evolution of the total heat flux (q_w) in Fig. 2 (left) shows larger increase in this quantity during the first transient for models-2 and 3 due to the larger value of D_v and this regardless of the heat transfer correlation. The steady state is obtained when the injected energy is balanced by the energy transferred from gas to wall and liquid phase. The heat exchange is then controlled by the imposed wall temperature and the constant thermodynamic conditions of the gas mixture. Thus, the total fluxes converge, for all HMT and D_v models, towards the same value (about $13.20\,\mathrm{kW/m^2}$). This value is lower than the injected enthalpy flowrate reported to wall surface ($\dot{m}\,h_{inj}/S_w = 13.60\,\mathrm{kW/m^2}$) due to the small rate of bulk condensation. A fast decrease in the value of the heat flux is observed at the end of steam injection leading

to thermal equilibrium between the gas mixture and the wall.

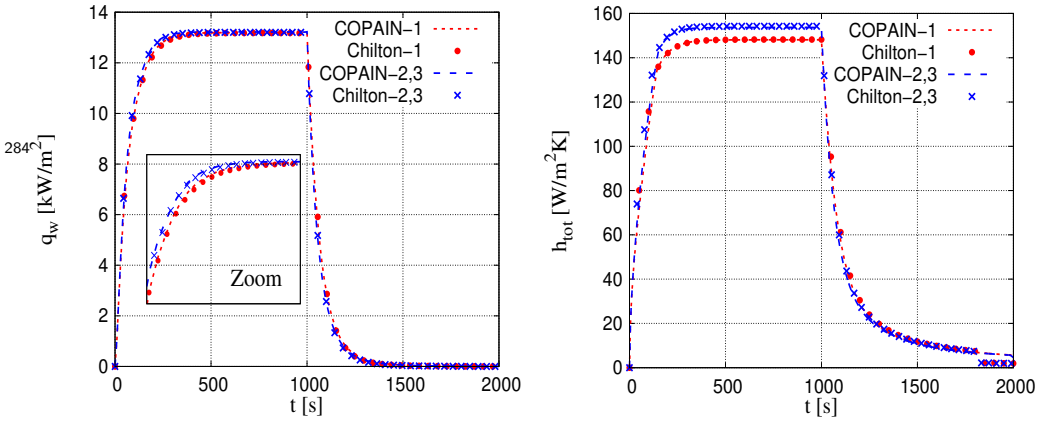

Figure 2: Test-1. Time evolution of the total heat flux (left) and the total heat transfer coefficient (right), using different models for HMT and D_v.

The respective contributions of condensation and convection heat fluxes are presented in Fig. 3 (left) and Fig. 3 (right). The condensation heat flux q_{cd}

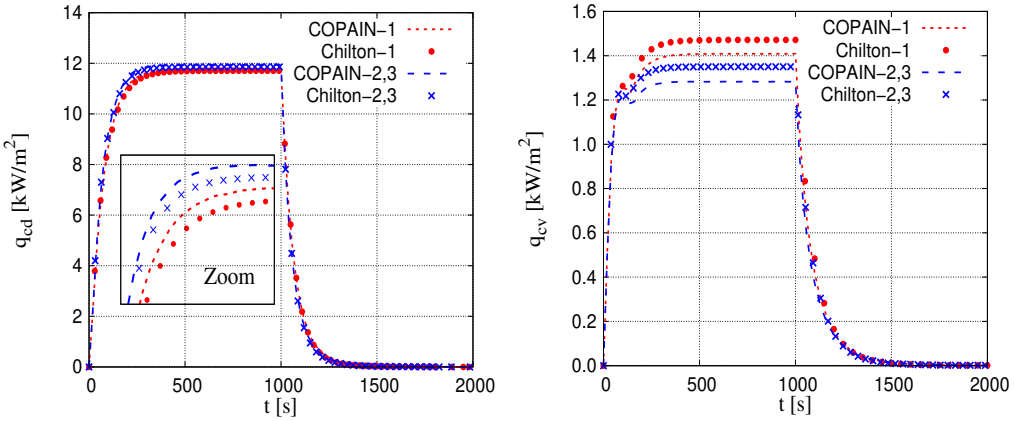

Figure 3: Test-1. Time evolution of the condensation heat flux (top) and the convection heat flux (down), using different models for HMT and D_v.

is more important for models-2 and 3 compared to model-1 due to the larger D_v which occurs with a power law exponent of 2/3 in the condensation heat flux formulation. COPAIN correlation gives a lightly larger q_{cd} compared to Chilton correlation. However, for the convective heat flux q_{cv}, which is one

order of magnitude lower than the condensation one, the trend is reversed which results in almost equal total heat fluxes.

Heat transfer coefficient. The total HTC given by model-1 is about 4% lower than that for model-2 and model-3 as shown in Fig. 2 (right).

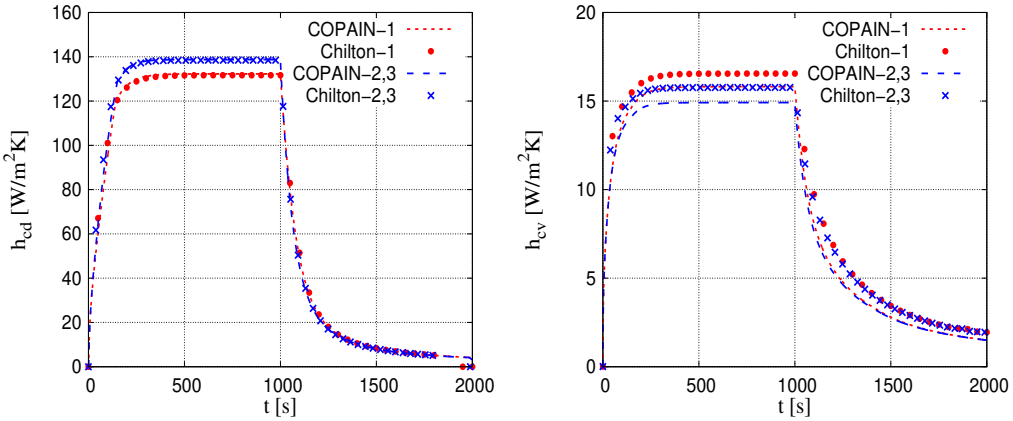

Figure 4: Test-1. Time evolution of the condensation HTC (left) and the convection HTC (right), using different models for HMT and D_v.

This implies that the wall-to-bulk temperature difference has an opposite behavior so as to balance the heat flux since $h_{tot} = q_w/(T_g - T_w)$. The sensitivity of the condensation HTC in Fig. 4 (left) to the D_v model and to the heat transfer correlation is similar to that of the total HTC while no influence is observed on the convective HTC Fig. 4 (right).

Temperature and steam molar fraction. At the early time of the steam injection (up to $t \sim 68\,\mathrm{s}$), the mean temperature in Fig. 5 (left) increases abruptly and reaches a peak resulting in superheated conditions of the gas mixture with higher values for COPAIN correlation irrespective of the D_v model. The peak of temperature is dumped by re-saturation of the gas mixture due to the continuously increasing steam content (see Fig. 5 right). In the steady state, the temperature obtained with model-1 of D_v is about 3℃ higher than that obtained with models-2 and 3 and this with a negligible influence of the HMT correlation.

Pressure and steam mass. Similar evolution is obtained for the pressure and the steam mass in Fig. 6 (left) and Fig. 6 (right) respectively. These two

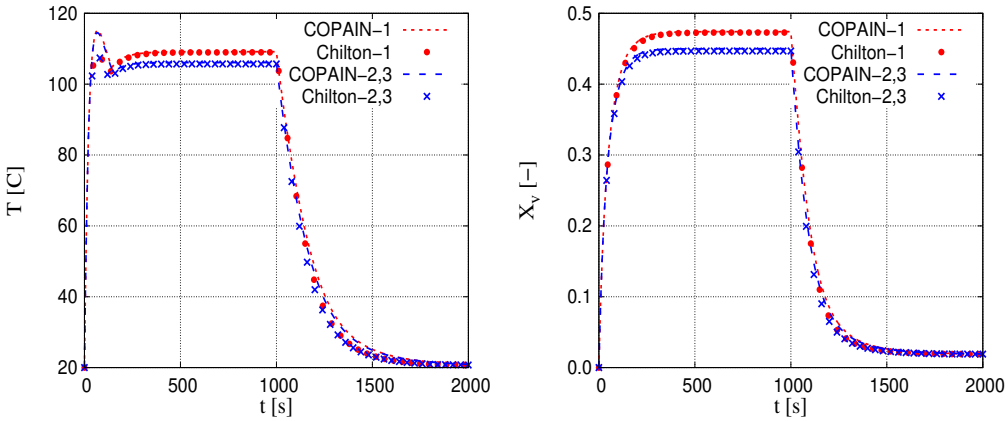

Figure 5: Test-1. Time evolution of the gas temperature (left) and the steam mass fraction(right) using different models for HMT and D_v.

quantities increase rapidly in the initial times as the steam is injected then stabilize to constant values when the injected energy is balanced by the energy transferred by condensation. At the end of injection, a sharp decrease is observed as for the gas temperature and the heat fluxes. The comparison

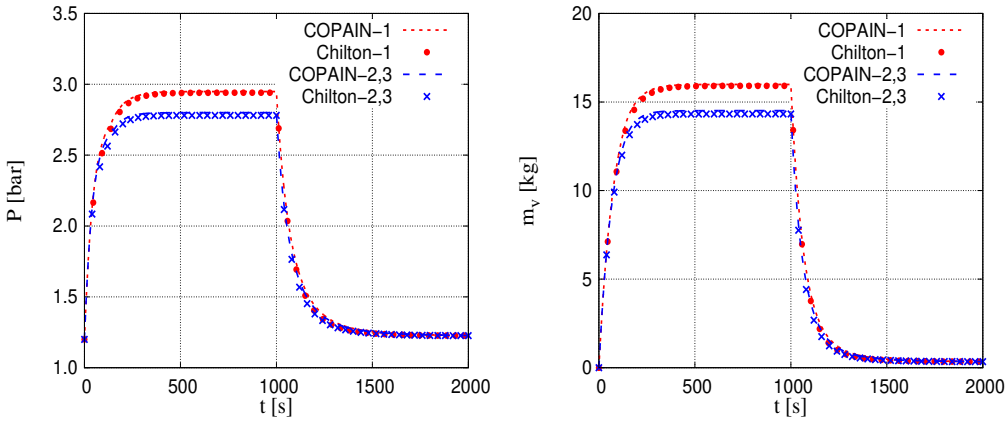

Figure 6: Test-1. Time evolution of the steam mass pressure (left) and the steam molar molar fraction (right) using different models for HMT and D_v.

of D_v and HMT models at the steady state, shows the same tendency as for the mean temperature but with stronger effect of the D_v modeling especially for the steam mass.

A quantitative comparison of the thermodynamic and heat transfer variables of test-1 is presented in table 4. To estimate the relative differences given in tables 4, 5, 7 and 8, we used as reference quantity the corresponding mean value except for the condensation and convection HTCs where the total heat transfer coefficient is used.

Variable	$\dot{m}_{cd}$ g/s	q_w kW/m^2	h_{tot} W/m^2K	h_{cd} W/m^2K	h_{cv} W/m^2K	P bar	T ℃	M_v kg
Average	191.0	13.200	151.04	135.29	15.75	2.867	107.49	15.18
Chilton-1	188.9	13.177	148.21	131.66	16.55	2.940	108.98	15.91
Chilton-2,3	191.8	13.210	154.21	138.47	15.75	2.781	105.72	14.32
COPAIN-1	190.2	13.194	148.08	132.27	15.81	2.949	109.17	15.99
COPAIN-2,3	193.0	13.220	153.68	138.76	14.91	2.799	106.1	14.51
Max err D_v %	1.5	0.2	4.0	4.5	0.6	5.6	3.0	10.5
Max err HMT %	0.7	0.1	0.4	0.4	0.6	0.7	0.3	1.2

Table 4: Comparison of the calculated quantities at the steady state. Relative errors to defined reference values.

Conclusion 1. As a conclusion for this test involving a binary mixture of steam and air, the influence of the D_v modeling on the global heat and mass transfer and consequently on the evolution of the containment thermodynamic conditions is significant compared to the effect of the HTM correlation. At the steady state, all models provide an equal total heat flux but the discrepancies in the transient due to different heat transfer coefficients result in different thermodynamic states of the atmosphere (pressure, temperature, mass, molar fractions). The wall condensation rate is smaller than injected steam flow rate. This difference is related to the bulk condensation which is less than 10%.

3.2. Multi-component mixture steam-air-hydrogen

3.2.1. Test-2: steam injection in air-hydrogen mixture

Test-2 differs from Test-1 in the initial composition of the gas mixture within the enclosure. Here, the atmosphere is composed of air and hydrogen with a hydrogen molar fraction of $X_{H_2} = 0.3$ and air molar fraction of $X_{air} = 0.7$ which results in a mass mixture of 21.10 kg. The initial pressure and

temperature of the atmosphere, the wall temperature and the steam injection conditions are the same as in Test-1.

3.2.2. Test-2 results

As for Test-1, calculations have been performed with Chilton and COPAIN correlations of heat and mass transfer where the effective diffusion coefficient D_v is determined separately with model-1, model-2 or model-3.

The effective diffusion coefficient. In the injection phase (see Fig. 7), higher values of D_v are obtained respectively for model-2, model-3 then model-1. This is explained by the contribution of the binary hydrogen-steam diffusion coefficient ($D_v^{H_2}$) when using molar fractions (model-2) instead of mass fractions (model-3). The low values of model-1 are explained by the steam self-diffusion coefficient contribution. In the post-injection phase, model-1 converges to model-3 as steam disappears. The effect of light gas

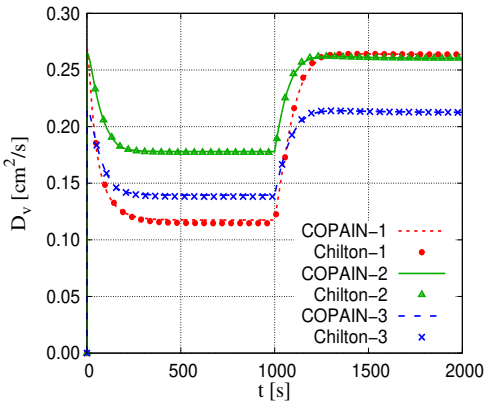

Figure 7: Test-2. Time evolution of the effective diffusion D_v using COPAIN and Chilton correlation with three different models for D_v.

(hydrogen) is highlighted by comparing test-1 and test-2 for the same model of HMT correlation. The results show that the presence of 30% of hydrogen leads to an increase of the effective diffusion coefficient of about 22% for model-2. One can expect that the model-3 provides D_v values close to that for the binary air-steam mixture of test-1 as shown in Fig. 1 due to the low hydrogen molecular weight. The HMT correlations have no impact on the effective diffusion coefficient evolution.

Heat flux. In accordance with D_v values, faster increase of the total heat flux (q_w) shown in Fig. 8 is observed respectively for model-2, model-3 and model-1 in the transient phase of steam injection. At the steady state, a constant average value of the heat flux is reached ($13.21\,\mathrm{kW/m^2}$) which is quite equal to that for test-1. Let's recall that, the injected enthalpy flowrate reported to wall surface is of $13.60\,\mathrm{W/m^2}$ and the difference is transferred by bulk condensation.

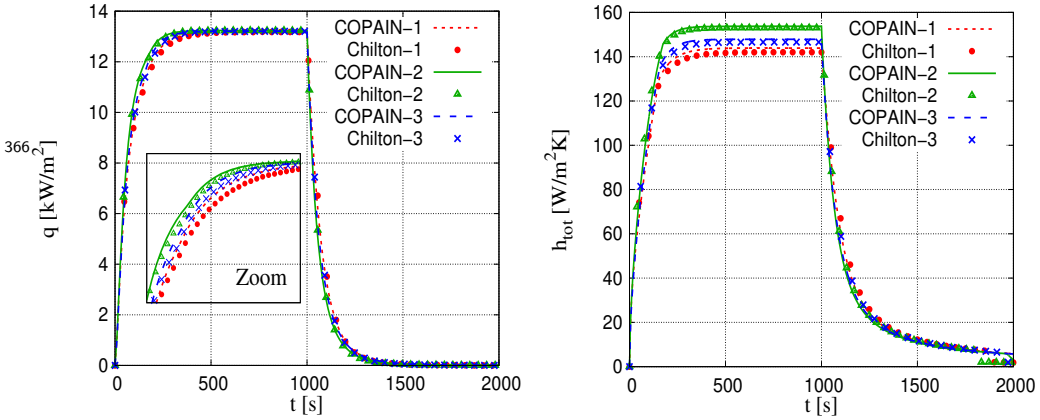

Figure 8: Test-2. Time evolution of the total heat flux (left) and the total heat transfer coefficient (right), using different models for HMT and D_v.

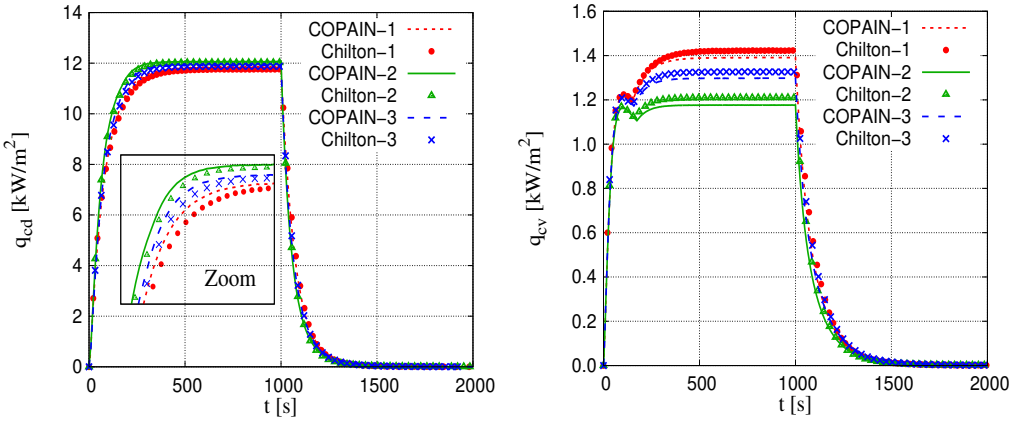

Figure 9: Test-2. Time evolution of the condensation heat flux (top) and the convection heat flux (down), using different models for HMT and D_v.

With regard to the respective contributions of condensation and convection heat transfers, the heat fluxes are compared in Fig. 9 (left) and Fig. 9 (right).

We notice an opposite behavior according to the HMT correlations and the D_v models resulting in almost equal total heat fluxes.

Heat transfer coefficient. Similar behavior according to the D_v and HMT models is obtained for the condensation and convection HTCs which is consistent with the respective heat fluxes contributions (see Fig. 10 left and Fig. 10 right).

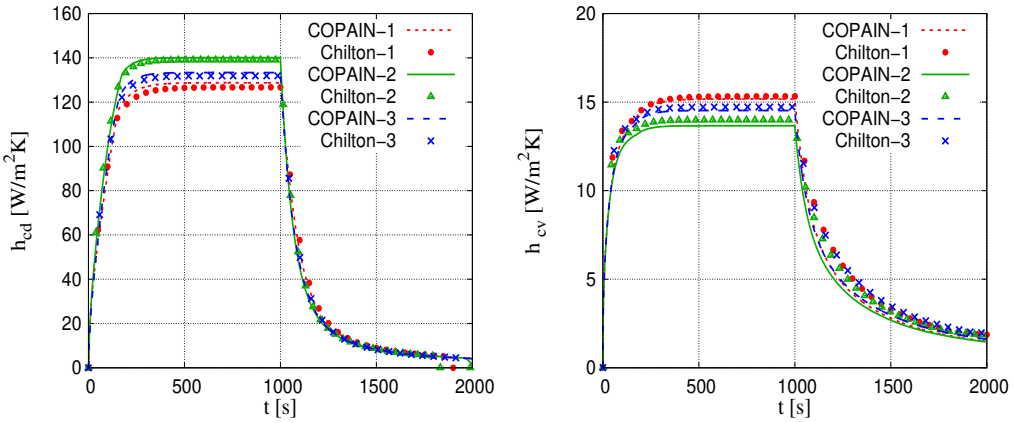

Figure 10: Test-2. Time evolution of the condensation HTC (top) and the convection HTC (down), using different models for HMT and D_v.

Temperature and steam molar fraction. As for test-1, superheated conditions are achieved at the early time of the steam injection (up to $t \sim 65\,\mathrm{s}$). Higher values of temperature are obtained for COPAIN correlation irrespective to the D_v model (see Fig. 11 (left)). The influence of the superheated gas temperature evolution on the convective heat fluxes is noticeable in Fig. 9 (right).

In the steady state associated to the saturation conditions, the higher is the total HTC, the lower is the temperature with clear distinction between model-2 and model-3 due to the effect of light gas. The impact of the D_v model on the gas temperature values is clearly more important than the effect of the HMT correlation. The evolution of the steam molar fraction in Fig. 11 (right) has the same behavior as temperature with respect to the HMT and D_v models at the steady state (the higher D_v is, the lower is X_v).

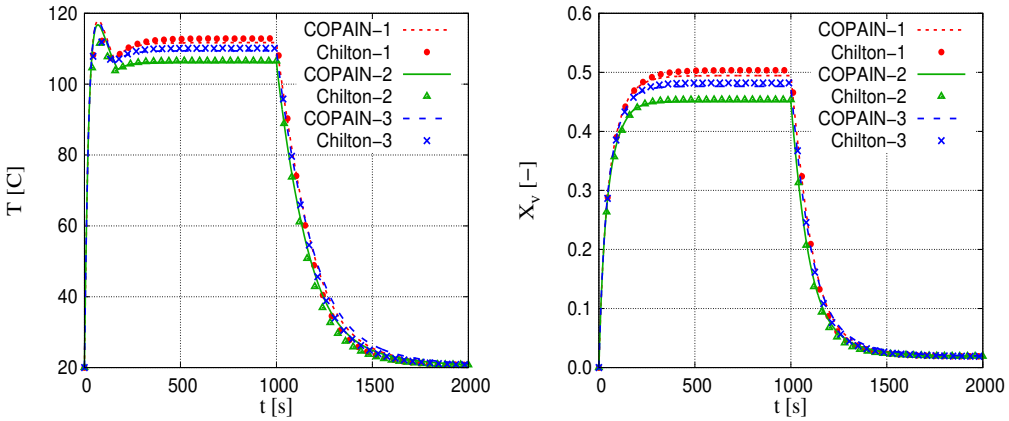

Figure 11: Test-2. Time evolution of the pressure and the steam mass using different models for HMT and D_v.

Pressure and steam mass. The pressure and the steam mass in Figs. 12 (left) and 12 (right) respectively have similar evolution. At the steady state, the comparison of D_v and HMT models shows the same tendency as for the mean temperature but with stronger effect of the D_v modeling.

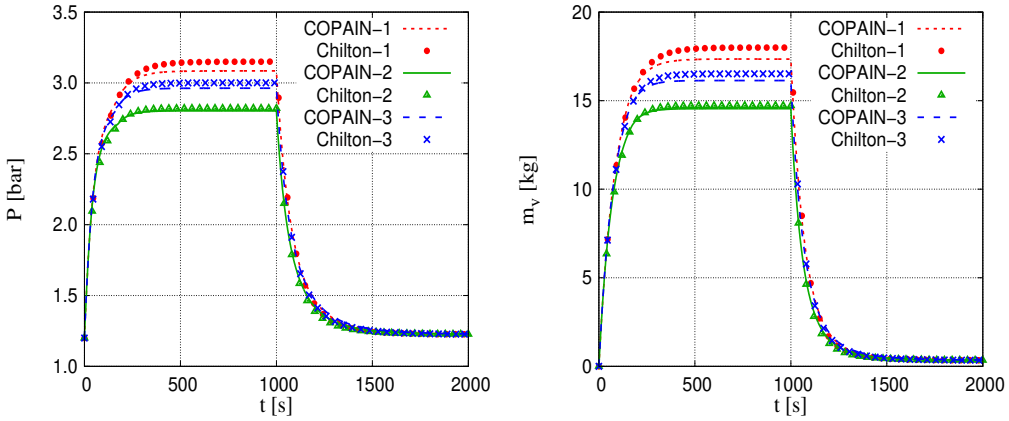

Figure 12: Test-2. Time evolution of : (left) the steam mass, (right) the steam molar fraction using different models for HMT and D_v.

Variable	$\dot{m}_{cd}$ g/s	q_w kW/m^2	h_{tot} W/m^2K	h_{cd} W/m^2K	h_{cv} W/m^2K	P bar	T ℃	M_v kg
Average	192.1	13.208	147.85	133.28	14.57	2.970	109.48	16.21
Chilton-1	189.3	13.178	142.03	126.70	15.33	3.150	112.86	18.00
Chilton-2	194.3	13.229	152.96	138.98	13.99	2.820	106.56	14.72
Chilton-3	191.6	13.202	146.63	131.89	14.74	3.001	110.15	16.52
COPAIN-1	190.2	13.191	143.89	128.73	15.16	3.085	111.74	17.35
COPAIN-2	195.0	13.235	153.72	140.07	13.67	2.804	106.17	14.54
COPAIN-3	192.3	13.212	147.86	133.32	14.54	2.963	109.40	16.13
Max err D_v %	2.6	0.4	7.4	8.3	1.0	11.1	5.8	20.2
Max err HMT %	0.4	0.1	1.3	1.4	0.2	2.2	1.0	4.0

Table 5: Comparison of the computed quantities at the steady state. Relative errors to defined reference values.

Conclusion 2. To conclude this analytic tests part, one can refer to table 5 for quantitative comparison. Test-2 involving a ternary mixture of steam, air and light gas (hydrogen) demonstrated the strengthened impact of the D_v formulation compared to the effect of HMT correlation on the global heat and mass transfer and on the containment atmosphere variables. Besides, test-2 revealed the impact of using mass or molar fractions in the effective D_v determination.

4. Validation test

The third test is the experimental exercise ISP-47 in MISTRA facility for the validation of the condensation modeling. The ISP47 test involves a ternary gas mixture of air-steam-helium where helium is used to simulate hydrogen leakage, see [27] for more details.

4.1. MISTRA facility

The MISTRA facility is dedicated to containment thermal-hydraulics and hydrogen risk assessment for nuclear reactors. MISTRA is a cylindrical stainless steel vessel of 97.6 m^3 of volume (figure 13). The internal diameter of 4.25 m and the height of 7.38 m were chosen to scale a typical french PWR containment with 0.1 length scale ratio. Three independent thermally

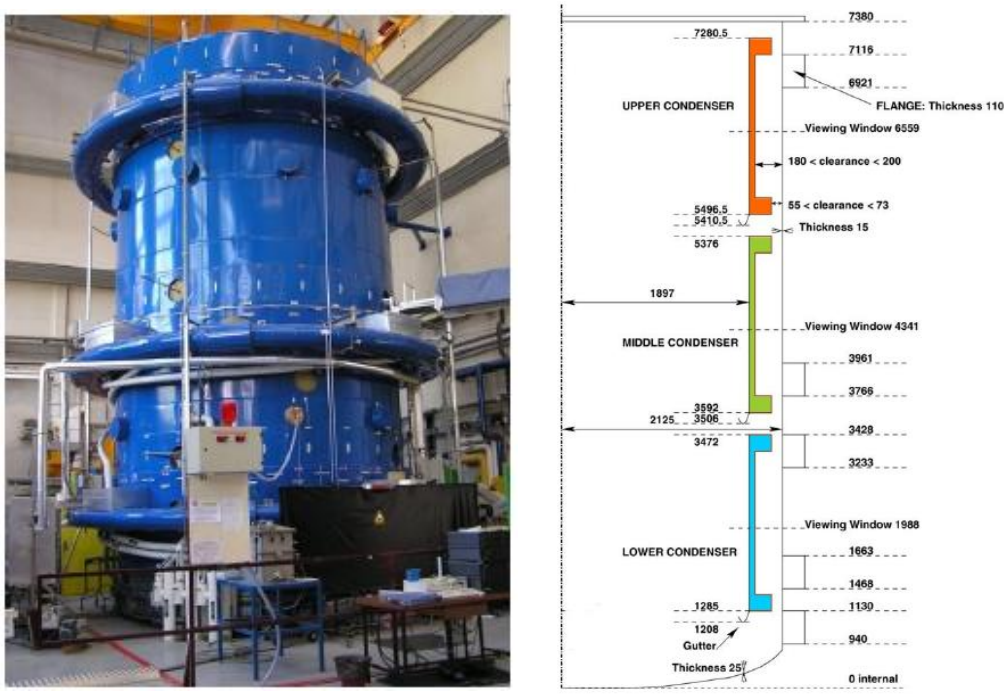

Figure 13: MISTRA facility: (left) external view, (right) schematic view with highlight on the condenser locations (dimensions in mm).

regulated walls, called condensers, are inserted inside the containment, close to the external wall, on top of each other. The external wall is thermally insulated with rock-wool layer of 20 cm thickness. A lower centered upward injection is set-up in this ISP-47 test.

4.2. ISP47-test description

The test sequence is divided into four successive phases with two steady-state conditions:

1. Preheating phase: superheated steam injection into the air-filled facility initially at room conditions in order to heat up the containment wall and the condensers and to generate initial homogeneous conditions ($P_0 = 1\,\text{bar}$, $T_0 = 20℃$). The steam is then injected continuously at 130 g/s mass flowrate and 200℃ during the test.
2. Air-steam steady state (Phase A) defined from the balance between the injected and condensed mass flows (130 g/s) ensuring the stability of

	Phase A Steam-air	**Phase B** Steam-air-helium	
	Steam	Steam	He
t(s)	45000	45000	1740
$\dot{m}$(g/s)	130	130	10.6
T(℃)	198-200	200	130-190

Table 6: Injection conditions of the MISTRA ISP47 test.

all the parameters: pressure, temperature and gas concentrations.

3. Air-steam-helium transient: helium (simulating hydrogen) mass flowrate of 10.6 g/s at 200℃ is added to the main steam during half an hour.
4. Air-steam-helium steady state (Phase B) with the same definition and boundary conditions as for Phase A.

Condensers are all maintained at the same temperature of 115℃ after the end of the preheating phase. It should be noticed that test-1 is represented by Phase A while test-2 is analogous to Phase B.

4.3. ISP47 test results

The ISP47-test simulations have been performed with one volume assuming a homogeneous atmosphere to avoid the effect of the nodalization scheme. For computations, imposed temperature is applied on condensers walls. On the other external walls, the temperature is determined by solving a 1-D conduction equation in the wall thickness. The heat exchange coefficient of the external walls with the environment is set to $5\,\mathrm{W/m^2K}$.

The effective diffusion coefficient. In Fig. 14, the effective diffusion coefficient D_v is represented over the entire duration of the test. The results confirm the trend observed for the analytic tests. In the first air-steam steady state, the D_v obtained with model-1 is about 33% lower than that in models 2 and 3 and this without any influence of the HMT correlation. Differences occur between the molar fraction weighted model (model-2) and the mass fraction one (model-3) in the second steady state following the helium injection. Moreover, unlike model-2, the helium injection does not affect the D_v evolution for model-1 because of the contribution of the steam self-diffion and for model-3 due to the small mass fraction of helium. Smaller differences related to the HMT correlation arise in this phase (B).

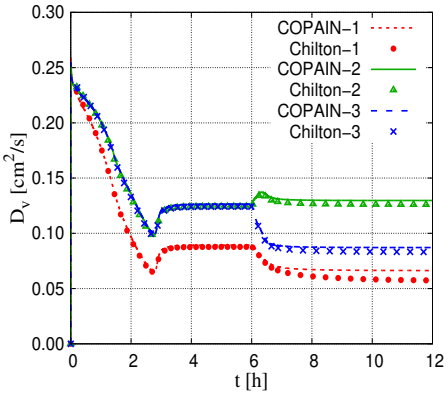

Figure 14: ISP47-test. Time evolution of the effective diffusion D_v using COPAIN and Chilton correlation with three different models for D_v.

Heat transfer flux and coefficients. The total heat fluxes exchanged on the imposed temperature walls (condensers) and the heat transfer coefficients are presented from the end of the preheating phase. At the first steady state,

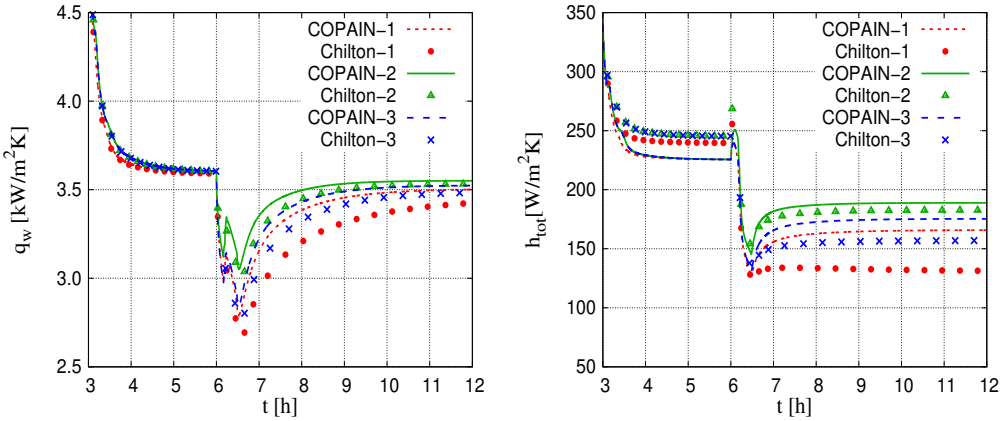

Figure 15: ISP47-test. Time evolution of the total heat flux (left) and the total heat transfer coefficient (right), on the condensers using different models for HMT and D_v.

involving the binary air-steam mixture in Fig 15 (left), the heat fluxes are almost all equal irrespective to the HMT or D_v modeling with a maximum relative difference of 0.3% as given in table 7. At the second steady state, the impact of D_v modeling is slightly growing to reach at most 4.3%. Note that, the heat flux calculated using Chilton correlation with model-1 (Chilton-1) is still evolving towards the steady state. The corresponding total heat transfer

coefficient is shown in Fig 15 (right).

As expected the condensation heat flux in figure 16 (left) has the same behavior of the total flux with comparable differences with respect to the HMT and D_v models. The convective heat flux in figure 16 (right) which is one order of magnitude lower than the condensation one is not influenced by the HMT correlation and not directly by the D_v modeling.

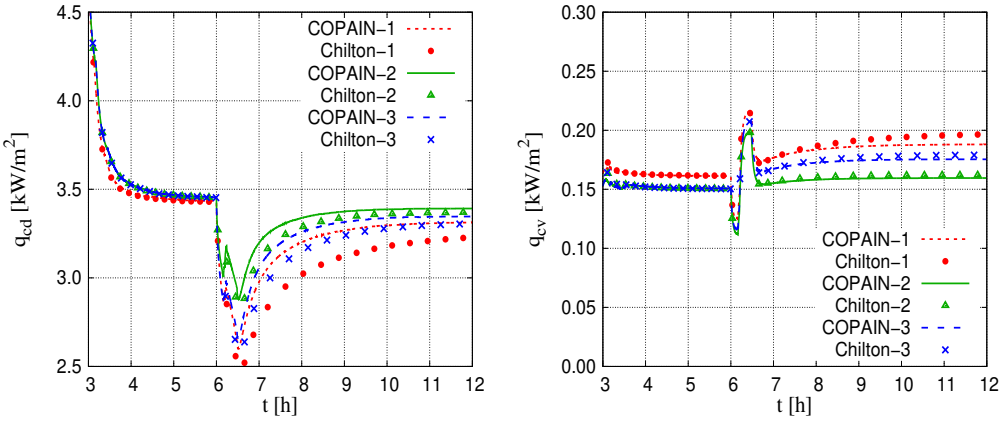

Figure 16: ISP47-test. Time evolution of the condensation HTC (left) and the convection HTC (right), on the imposed-temperature walls using different models for HMT and D_v.

Pressure and temperature. The calculated pressure and temperature evolution are compared to experimental results in Fig. 17 (left) and (right) respectively. Note that, the experimental temperature is measured at the upper part of the MISTRA containment ($z = 7.2\,\mathrm{m}$), a priori higher than the experimental averaged temperature. For all HMT and D_v models, calculations correspond generally to the experimental evolution. In the first steady state (air-steam), the pressure is slightly overestimated compared to the measurements and little more when model-1 for D_v is used. For the temperature all models give the same results about 5°C above the experimental one.

In the air-steam-helium steady state, except for model-2 for D_v, increasing differences with the measured pressure and temperature are observed especially for Chilton correlation with model-1.

Steam mass and molar fraction. The steam mass evolution in Figs 18 (left) is very similar to the pressure. Large differences between models appear on the steam mass only for the air-helium-steam phase. Note that, in this last

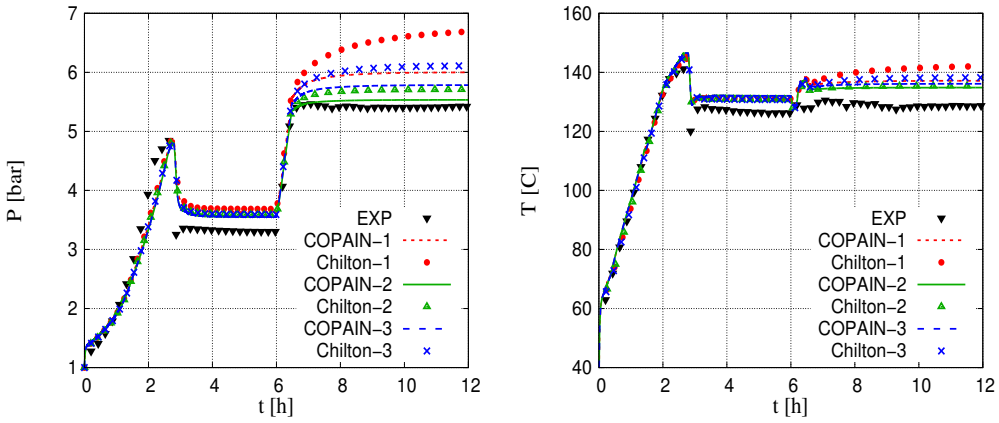

Figure 17: ISP47-test. Time evolution of the experimental and calculated pressure (left) and temperature (right) using different models for HMT and D_v.

phase, model-1 involving the steam self-diffusion coefficient underestimates significantly the condensation rate especially for Chilton correlation, resulting in larger steam amount. Concerning the molar fraction evolution 18 (right), the helium injection leads to a large decrease of this quantity. The impact of the D_v is similar to that on steam mass with less relative differences due to light gas effect.

From the quantitative point of view, the impact of D_v modeling is more important than the HMT correlation one (see tables 7 and 8). In table 9, the computed results have been compared against the experimental measurements of the pressure at the steady states. The relative errors are defined as $(P - P_{exp})/P_{exp}$ and $(\dot{m}_{cd} - \dot{m}_{cd\,exp})/\dot{m}_{cd\,exp}$

Conclusion 3. This last experimental test corroborate the conclusions of the analytic test-1 and test-2 represented here by phases A and B respectively. For this scenario, the impact of D_v modeling remains higher than the effect of the HTM correlation even if the COPAIN correlation is less sensitive than the Chilton one. The model-2 is the closest to the experimental results independently of the HTM correlation. Furthermore, by taking into account the steam self-diffusion in D_v formulation, the steam condensation is significantly reduced by model-1 in presence of a light gas.

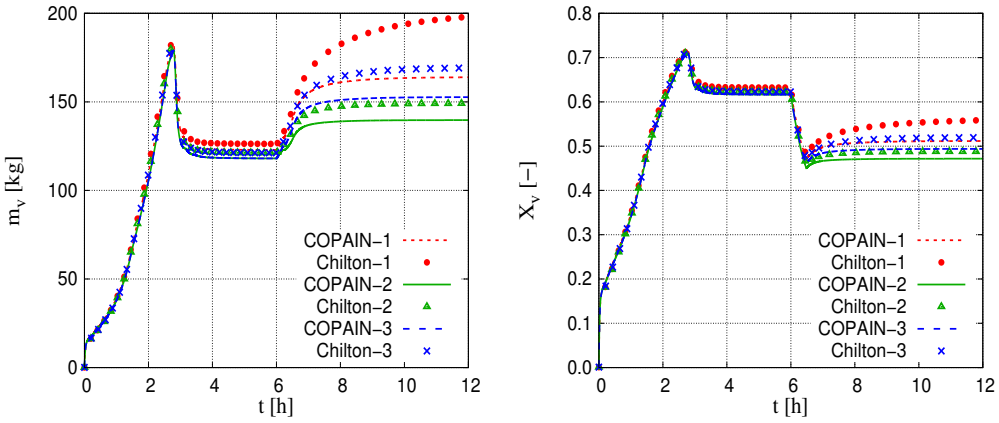

Figure 18: ISP47-test. Time evolution of the steam mass (left) and the steam molar fraction (right) using different models for HMT and D_v.

Variable	$\dot{m}_{cd}$ g/s	q_w kW/m^2	h_{tot} W/m^2K	h_{cd} W/m^2K	h_{cv} W/m^2K	P bar	T ℃	M_v kg
Reference	106.2	3.601	234.50	224.46	10.04	3.599	131.44	121.29
Chilton-1	105.8	3.591	239.61	228.82	10.79	3.685	131.05	126.28
Chilton-2,3	106.5	3.604	245.33	235.09	10.24	3.591	130.75	121.22
COPAIN-1	105.8	3.595	225.54	215.41	10.13	3.633	131.99	122.86
COPAIN-2,3	106.4	3.606	225.60	216.18	9.42	3.548	132.04	118.06
Max err D_v %	0.7	0.3	2.4	2.7	0.3	2.6	0.2	4.2
Max err HMT %	0.1	0.1	8.4	8.1	0.3	1.4	1.2	2.8

Table 7: ISP47-test. Comparison of the calculated quantities at the end of phase A (air-steam mixture).

5. Conclusion

The aim of this work is the assessment of heat and mass transfer correlations for condensation in presence of noncondensable gases including light gas. Particular attention is paid to the modeling of the effective diffusion coefficient. The presence of light gas such as hydrogen is representative of accidental situation in nuclear reactor.

We addressed correlations for film condensation based on the diffusion

Variable	$\dot{m}_{cd}$ g/s	q_w kW/m^2	h_{tot} W/m^2K	h_{cd} W/m^2K	h_{cv} W/m^2K	P bar	T ℃	M_v kg
Reference	102.3	3.505	166.79	158.46	8.33	5.974	137.32	162.20
Chilton-1	99.3	3.433	131.18	123.76	7.34	6.705	142.19	198.60
Chilton-2	103.7	3.532	182.65	174.31	8.34	5.710	135.38	149.11
Chilton-3	101.6	3.486	156.91	148.87	8.05	6.111	138.24	169.13
COPAIN-1	101.9	3.503	165.67	156.90	8.77	5.999	137.15	163.93
COPAIN-2	104.3	3.551	188.93	180.35	8.58	5.532	134.84	139.77
COPAIN-3	103.0	3.524	175.37	166.55	8.82	5.785	136.14	152.64
Max err D_v %	4.3	2.8	30.9	30.3	0.5	16.7	5.0	30.5
Max err HMT %	2.6	2.0	20.7	19.9	0.8	11.8	3.7	21.4

Table 8: ISP47-test. Comparison of the calculated quantities at the end of phase B (air-steam-helium mixture).

	Phase A Steam-air				Phase B Steam-air-helium			
	P(bar)	$\frac{\lvert\Delta P\rvert}{P_{ex}}$	$\dot{m}_{cd}$(g/s)	$\frac{\lvert\Delta\dot{m}_{cd}\rvert}{\dot{m}_{ex}}$	P(bar)	$\frac{\lvert\Delta P\rvert}{P_{ex}}$	$\dot{m}_{cd}$(g/s)	$\frac{\lvert\Delta\dot{m}_{cd}\rvert}{\dot{m}_{ex}}$
Experiment	**3.300**	-	**116.6**		**5.405**	-	**113.5**	-
Chilton-1	3.685	11.7 %	105.8	9.28 %	6.705	24.0 %	99.3	12.5 %
Chilton-2	3.591	8.83 %	106.5	8.74 %	5.710	5.64 %	103.7	8.64 %
Chilton-3	3.591	8.83 %	106.5	8.74 %	6.111	13.1 %	101.6	10.4 %
COPAIN-1	3.633	10.1 %	105.6	9.27 %	5.999	11.0 %	101.9	10.2 %
COPAIN-2	3.548	7.51 %	106.4	8.65 %	5.532	7.04 %	104.3	8.09 %
COPAIN-3	3.548	7.51 %	106.4	8.65 %	5.785	13.1 %	103.0	9.27 %

Table 9: Comparison of the computed and experimental pressure and condensation flowrate on the condenser walls.

layer theory using heat and mass transfer analogy. The so-called Chilton and COPAIN correlations have been evaluated with several models for the effective diffusion coefficient. For this purpose, two simplified test-cases consisting of steam injection into an enclosure initially filled with air for Test-1 and with air-hydrogen mixture for Test-2 have been investigated. The validation was carried out using the experimental international standard

problem ISP-47 performed in MISTRA facility. This test comprises a first phase with a binary air-steam mixture and a second phase involving light gas with air-steam-helium mixture.

For all cases, the D_v model including the steam self-diffusion leads to an underestimation of the heat and mass transfer. This is due to the decrease of the steam self-diffusion coefficient which is inversely proportional to the pressure regardless of the temperature. This results in larger values of pressure and temperature compared to the D_v models involving only noncondensable gases. The comparison with the ISP47 experimental results showed that the Chilton and COPAIN correlations underestimate the condensation rate in the steady state. Besides, the effective diffusion coefficient based on molar fractions instead of mass fraction provides more accurate predictions of the physical quantities.

Furthermore, it has been shown that the influence of the D_v modeling on the heat and mass transfer is significant compared to the effect of the heat and mass transfer correlation. This is particularly true in the presence of light gas. As a result, this work brought out the importance of the modeling of the relevant parameters involved in heat and mass transfer correlations.

In future work, it would be worth investigating the effect of the effective diffusion coefficient modeling at the CFD scale.

Appendix A. Summary of previous work: some experimental and theoretical models

Author	Total HTC	Film HTC	Condensation HTC	Convective HTC
Experimental				
Uchida [9]	$h = 379 \left(\frac{Y_{v,b}}{Y_{nc,b}} \right)^{0.707}$			
Tagami [10]	$h_{steady} = 11.356 + 283.9 \left(\frac{Y_{v,b}}{Y_{nc,b}} \right)$			
Dehbi[11]	$h = \frac{L^{0.05}(3.7 + 28.7P) - (2438 + 458.3P) \log Y_{nc,b}}{(T_b - T_w)^{0.25}}$			
Theoretical				
Peterson [21]	$h = h_{cd} + h_{cv}$		$h_{cd} = 0.1(\mathrm{Gr}\,\mathrm{Sc})^{1/3} \frac{\lambda_{cd}}{L}$, $\lambda_{cd} = \frac{X_{v,ave}}{X_{nc,ave}} \frac{h_{fg}^2 P\, D}{R_v^2 T_{ave}^3}$	$h_{cv} = 0.7(\mathrm{Gr}\,\mathrm{Pr})^{1/3} \frac{\lambda_g}{L}$
Herranz [22]	$h = \frac{1}{\frac{1}{h_f} + \frac{1}{h_{cd} + h_{cv}}}$	$h_f = \mathrm{Re}_l^{0.04} \left(\frac{g \rho_l (\rho_l - \rho_v) h'_{fg} \lambda_l^3}{\mu_l (T_i - T_w) L} \right)^{1/4}$	$h_{cd} = \frac{\mathrm{Sh}\, \lambda_{cd,mod}}{L}$, $\lambda_{cd,mod} = \frac{X_{v,ave}}{X_{nc,ave}} \frac{C \bar{h}_{fg}^2 W_v\, D}{R_v T_i\, T_b}$	$h_{cv} = 0.13(\mathrm{Gr}\,\mathrm{Pr})^{1/3} \frac{\lambda_g}{L}$
Dehbi [25]	$h = C_g . D^{2/3} (\rho_w + \rho_b) \frac{(\rho_w - \rho_b)^{1/3} h_{fg}}{\mu^{1/3} (T_b - T_w)} \ln \frac{Y_{nc,w}}{Y_{nc,b}}$ air-steam: $C_g = 0.185$, air-steam-He: $C_g = 0.163$			

Table A.10: Summary of previous work: some experimental and theoretical models.

References

[1] W. Nusselt, The condensation of steam on cooled surfaces, Z. d. Ver. Deut. Ing. 60 (1916) 541–546, (Translated into English by D. Fullarton, *Chem. Engr. Funds.*, 1(2):6–19, 1982).

[2] L. Bromley, Effect of heat capacity of condensate, Ind. Eng. Chem 44 (1952) 2966–2969.

[3] W. M. Rohsenow, Heat transfer and temperature distribution in laminar film condensation, Trans. Am. Soc. Mech. Eng. 78 (1956) 1645–1648.

[4] E. Sparrow, J. Gregg, A boundary-layer treatment of laminar film condensation, Heat Transfer Series 81 (1959) 13.

[5] J. Koh, E. Sparrow, J. Hartnett, The two phase boundary layer in laminar film condensation, International Journal of Heat and Mass Transfer 2 (1961) 69–82.

[6] E. Sparrow, S. Lin, Condensation heat transfer in the presence of noncondensables gas, Journal of Heat and Mass Transfer C86 (1964) 430–436.

[7] W. Minkowycz, E. Sparrow, Condensation heat transfer in the presence of noncondensables, interfacial resistance, superheating, variable properties, and diffusion, International Journal of Heat and Mass Transfer 9 (1966) 1125–1144.

[8] J. Rose, Condensation of a vapor in the presence of a non condensing gas, Intetnational Journal of Heat and Mass Transfer 12 (1969) 233–237.

[9] H. Uchida, A. Oyama, Y. Togo, Evaluation of post-accident cooling systems of LWR's, 93-102 (1965).

[10] H. Fujie, A. Yamanouchi, N. Sagawa, H. Ogasawara, T. Tagami, Studies for safety analysis of loss-of-coolant accidents in light-water power reactors, J. Japan Soc. Mech. Engrs. 69 (571) (1966) 1068–1076.

[11] A. Dehbi, M. Golay, M. Kazimi, Condensation experiments in steam-air and steam-air-helium mixtures under turbulent natural convection, 1991, pp. 19–28.

[12] T. Chilton, A. P. Colburn, Evaporation of water into a laminar stream of air and superheated steam, Industrial and Engineering Chemistry 26 (1934) 373–380.

[13] R. Bird, W. Stewart, E. Lightfoot, Transport phenomena, Wiley ed, 1960.

[14] J. Collier, J. Thome, Convective Boiling and Condensation, McGraw-Hill Book Compagny, UK, 1972.

[15] D. Spalding, A standard formulation of the steady mass transfer problem, International Journal of Heat and Mass Transfer 1 (60) 192–207.

[16] D. Butterworth, G. Hewitt, Two-phase flow and heat transfer, Oxford University Press., Oxford. 1977.

[17] R. Whitley, Condensation heat transfert in a pressurized water reactor dry containment following a loss of coolant accident, Ph.D. thesis, University of California at Los Angeles (1976).

[18] M. Corradini, Turbulent condensation on cold wall in the presence of a noncondensable gas, Heat Transfer and Fluid Flow 64 (1984) 186–195.

[19] M. Kim, , M. Corradini, Modeling of condensation heat transfer in reactor containement, Nuclear Engineering and Design 118 (1990) 193–212.

[20] P. Peterson, V. Schrock, T. Kageyama, Diffusion layer theory for turbulent vapor condensation with noncondensable gases, Journal of Heat and Mass Transfer 115 (1993) 998–1003.

[21] P. Peterson, Theoretical basis for the Uchida correlation for condensation in reactor containments, Nuclear Engineering and Design 162 (1996) 301–306.

[22] L. Herranz, M. Anderson, M. Corradini, A diffusion layer model for steam condensation within the ap600 containment, Nuclear Engineering and Design 183 (1998) 133–150.

[23] P. Bazin, P. Castelli, COPAIN Rapport d'essais, Internal report DTP/SETEX/LETS/99-85, CEA (1999).

[24] A. Dehbi, A generalized correlation for steam condensation rates in the presence of air under turbulent free convection, International Journal of Heat and Mass Transfer 86 (2015) 1–15.

[25] A. Dehbi, A unified correlation for steam condensation rates in the presence of air-helium mixtures under naturally driven flows, Nuclear Engineering and Design 300 (2016) 601–609.

[26] J. W. Martin-Valdepeñas, M. Jimenez, F. Martin-Fuertes, J. Fernandez, Improvements in a CFD code for analysis of hydrogen behaviour within containments, Nuclear Engineering and Design 237 (2007) 627–647.

[27] E. Studer, J.-P. Magnaud, F. Dabbene, I. Tkatschenko, International standard problem on containment thermal-hydraulics ISP47 step 1 — results from the MISTRA exercise, Nuclear Engineering and Design 237 (2007) 536–551.

[28] W. Rohsenow, Y. Choi, Heat, mass and momentum transfer (1961).

[29] R. Moffat, W. Kays, The turbulent boundary layer on a porous plate: experimental heat transfer with uniform blowing and suction, International Journal of Heat and Mass Transfer 11 (1968) 1547–1566.

[30] RALOC, Mod4.0, Tech. rep., GRS, reference Manual (1996).

[31] S. Benteboula, Etude bibliographique des modèles de condensation en paroi pour une application à l'enceinte de confinement, Internal report STMF/LATF/NT/2018-62726/A, CEA (2018).

[32] S. Benteboula, F. Dabbene, Nodalization schemes for lumped-parameter calculations of representative nuclear reactor severe accident tests in the MISTRA facilty, in: Proc. In: 16^{th} International Topical Meeting on Nuclear Reactor Thermalhydraulics, NURETH-16, Chicago, USA, August 30-September 4, 2016.

[33] A. Dehbi, S. Kelm, J. Kalilainen, H. Mueller, The influence of thermal radiation on the free convetion inside enclosures, Nuclear Engineering and Design 341 (2019) 176–185.

[34] X. Cheng, P. Bazin, P. Cornet, D. Hittnerd, J. Jacksone, A. N. J Lopez Jimenez, F. Oriolo, H. Petzold, Experimental data base for

containment thermalhydraulic analysis, Nuclear Engineering and Design 204 (2001) 264–284.

[35] C. Wilke, C. Lee, Estimation of diffusion coefficients fot gases and vapors, Ind. Eng. Chem 47 (1955) 1253–1257.

[36] J. W. Martin-Valdepeñas, M. Jimenez, F. Martin-Fuertes, J. Fernandez, Comparison of film condensation models in presence of non-condensable gases implemented in a CFD code, Heat Mass Transfer 41 (2005) 961–976.

[37] R. Kee, G. Dixon-Lewis, J. Warnatz, M. Coltrin, J. Miller, A Fortran computer code package for the evaluation of gas-phase multicomponent transport properties, SANDIA Report SAND86-8246 (1986).

[38] B. Poling, J. Prausnitz, J. O'Connell, The properties of gases and liquids, Mc GrawHill, Fifth edition, 2001.